ACS APPLIED ENERGY MATERIALS

www.acsaem.org Article

Efficiency and Stability Enhancement of Perovskite Solar Cells Utilizing a Thiol Ligand and MoS_2 (100) Nanosheet Surface Modification

Masoud Karimipour,* Sepideh Khazraei, Byeong Jo Kim, Gerrit Boschloo, and Erik M. J. Johansson*

Cite This: *ACS Appl. Energy Mater.* 2021, 4, 14080−14092 Read Online

ACCESS | Metrics & More | Article Recommendations | Supporting Information

ABSTRACT: Surface modification of perovskite films using a combination of 1-dodecanethiol (DT) and MoS_2 nanosheets is investigated for perovskite solar cells. This surface modification is studied for two different types of perovskites, one with triple cations (CsFAMA) and one with double cations (FAMA), resulting in solar cell devices with power conversion efficiency (PCE) values of 18−19 and >20%, respectively. In both cases, stability enhancement is observed with DT and MoS_2 surface modification using three different stability tracking protocols. The results reveal that by including DT and MoS_2, the device retains 92% of its highest efficiency after 2200 h in dark (in air), while the standard device retained only 72%. Moreover, after light cycling, the device with DT and MoS_2 retained 80%, and the standard device retained 55% of its maximum PCE. Moreover, these surface modifications gave rise to 58% decrease in the number of short-circuited devices and more reproducible results. Different characterizations revealed that the stability and efficiency enhancement is mainly due to reduced interface trap densities, improved charge transfer, and longer charge carrier lifetime. Moreover, the DT and MoS_2 modifications induce hydrophobicity with an average contact angle over 80°.

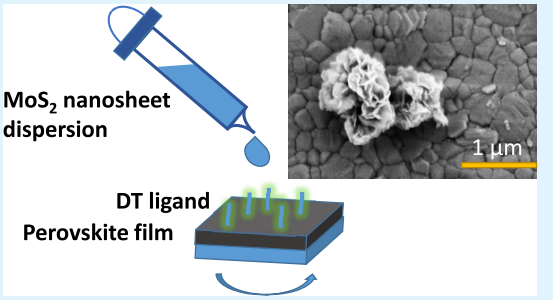

KEYWORDS: *perovskite solar cells, surface modification, ligand bridging, MoS_2 nanosheets, impedance spectroscopy, stability protocol, trap density*

1. INTRODUCTION

Metal halide perovskite solar cells with different layering and structures have opened a wide and diverse area of research due to their promising optoelectronic properties in the field of photovoltaic applications in the last decade. They are highly promising to be considered the next generation of commercial solar cells with cheap and affordable cost of raw materials and preparation technology.[1−9] Although there have been great successes and deep understanding in the different aspects of photovoltaic performance of perovskite solar cells, they still suffer from low stability and durability under the working conditions.[10−14] This instability rises from the thermal instability of the perovskites, observable hysteresis in their *J*−*V* measurements, hydrophilicity and moisture decomposition, cation and anion migrations, and interaction with the interfaces.[15−20] Most of the reports relate the hysteresis effects to the interface effects between the electron transport layer (ETL) and perovskite interface.[20,21] Thus, the passivation of ETL/perovskite has been the focus of many research studies to reveal the effect of surface passivation and ion migrations for achieving highly stable devices.[22−24] On the other hand, the study of different hole transport layers (HTLs) different from Spiro-OMeTAD as the most efficient HTL[25−28] has been mainly based on their degree of hydrophobicity, doping effects, and efficient and cost-effective hole transfer material. However, to implement many of the new suggested HTLs, some new ETL layers should be added in the layering process to compensate the band offsets[29] or even the device structure should be changed from n−i−p to p−i−n which imposes extra layering and interface concerns and modifications. On the other hand, Spiro-OMeTAD has been widely used as conventional HTL for the different types of perovskite compositions despite its high cost. This is because, first, it has a well-aligned valence band position (−5.2 eV) with respect to many types of lead perovskite valence bands ranging from −5.9 to −5.4 eV and different back contacts,[30] second is the simplicity of its solution preparation and deposition on the perovskite layer, and third is its high current density throughput.[30] However, due to its low crystallization temperature and tendency of interaction with the perovskite layer,[30] its application as HTL in long-term stable photovoltaics is still controversial.[31,32] Thus, the passivation of the perovskite/HTL

Received: September 14, 2021
Accepted: November 27, 2021
Published: December 8, 2021

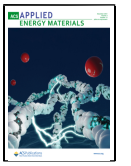

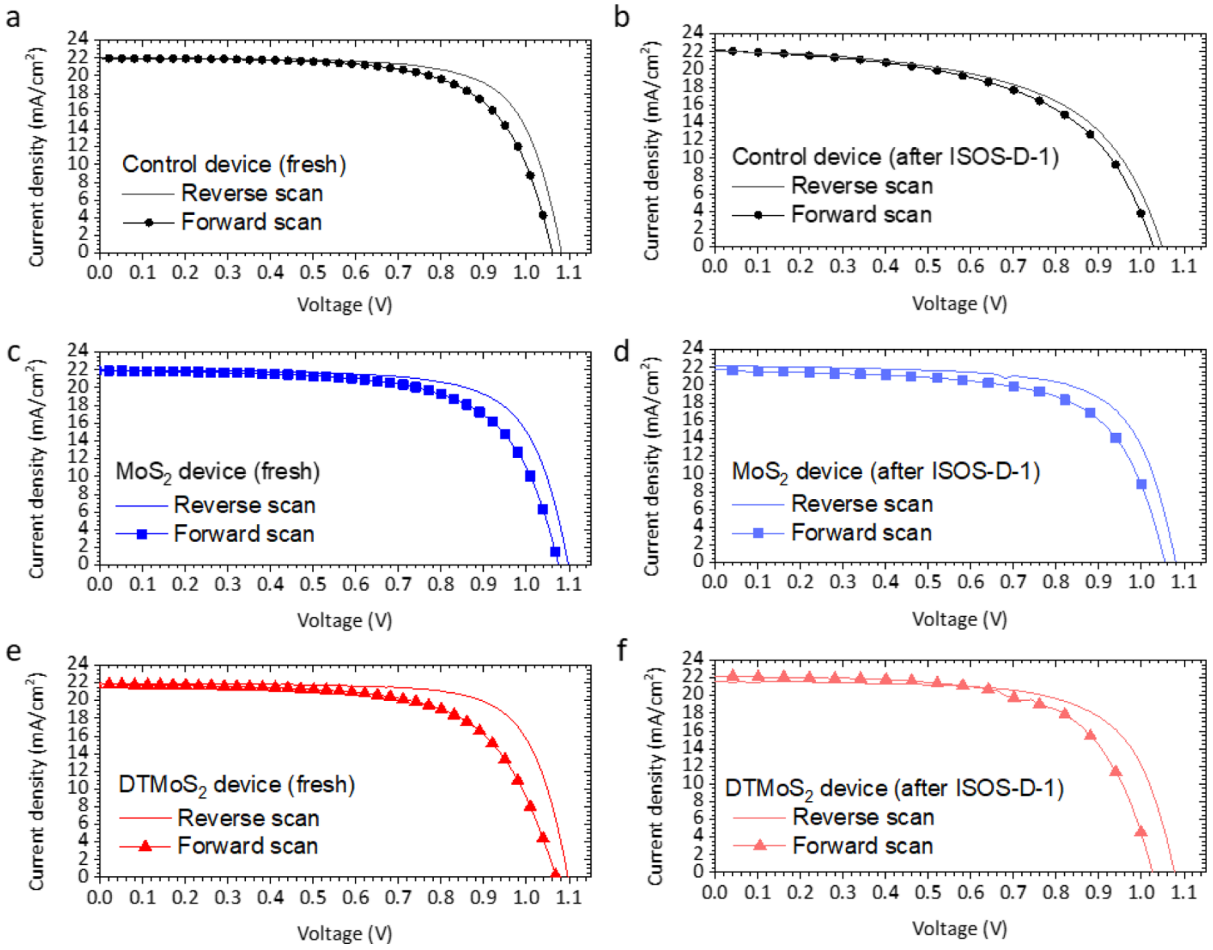

Figure 1. Reverse−forward *JV* measurements for (a), (b) fresh and aged (ISOS-D-1) control device, (c), (d) fresh and aged (ISOS-D-1) MoS_2-treated device and (e), and (f) fresh and aged (ISOS-D-1) $DTMoS_2$-treated device, respectively. ISOS-D-1 is the protocol for stability check, keeping samples in dark and a N_2 atmosphere with sequential measurements in an ambient atmosphere. CsFAMA perovskite was used for the fabrication of these devices.

interface has also been done by varieties of interfacial engineering methods, such as two-dimensional perovskite layers,[33] ligand-based modification,[34] or even inorganic materials.[9] One of the candidates as inorganic HTL for efficient hole transport is two-dimensional (2D) chalcogenide MoS_2 nanosheets.[35] MoS_2 few-layered nanosheets have been reported to be applied as HTL in normal n−i−p planar structure by Capasso et al.[36] According to this report, MoS_2 was used as a compact layer to enhance both the shunt resistance between the perovskite and Au contact as well as an efficient hole transfer layer.[36] Moreover, it was found that MoS_2 increases the stability of the device, although the efficiency (13.09%) was not superior to the reference device.[36] In another report, Dai et al. have mixed MoS_2 nanosheets with a conductive polymer PEDOT:PSS [poly(3,4-ethylenedioxythiophene) polystyrene sulfonate], leading to a significant enhancement of the performance of planar perovskite solar cells up to 16.47%.[37] In another report, Wang et al. have also mixed MoS_2 nanosheets with PEDOT:PSS as HTL in the p−i−n structure and have obtained an efficiency enhancement of 18.14% compared to the reference report.[38] Najafi et al. applied MoS_2 quantum dots/graphene hybrids in a mesoporous $MAPbI_3$ ($CH_3NH_3PbI_3$)-based n−i−p structure with Spiro-OMeTAD as the HTL to achieve an efficiency of 20.12% for their champion device.[39] They have homogenized the deposition of HTLs by chemical silanization linkage between reduced graphene oxide and (3-mercaptopropyl) trimethoxysilane to reduce pin holes due to MoS_2 quantum dot deposition.[39] Despite the successful reports on the application of MoS_2 nanostructures, the type of perovskite applied for achieving high efficiencies is limited to $MAPbI_3$ in all the reports.[35−39] This rise from the energy diagram point of view is because only the valence band of $MAPBI_3$ (−5.4 eV) well matches the valence band of MoS_2 (−5.1 eV) and Spiro-OMeTAD (−5.2 eV). Moreover, the application of lone MoS_2 as a complete layer mostly results in low open circuit voltages.[36,39]

In this work, we employ MoS_2 nanosheets to increase the stability, fill factor (FF), and performance of perovskite solar cells by deposition of a colloidal solution of MoS_2 nanosheets on different perovskite compositions cesium formamidinium methylammonium (CsFAMA triple cations) and formamidinium methylammonium (FAMA double cations). We show that the colloidal MoS_2 nanosheets enhance the stability of the devices while maintaining the V_{OC} values of the device. In addition to that, we employ a thiol-based ligand modification for better linkage between the MoS_2 nanosheets and the perovskites to further enhance charge transfer and device performance. We find that this surface modification using MoS_2 nanosheets can be employed for different types of

https://doi.org/10.1021/acsaem.1c02412
ACS Appl. Energy Mater. 2021, 4, 14080−14092

perovskites and that it shows promising results for achieving increased stability of the lead halide perovskite solar cells.

2. RESULTS AND DISCUSSION

The main idea of the current study is to employ MoS_2 nanosheets not as mere HTL[39] but as a modifier of the perovskite surface in perovskite solar cells to increase charge extraction from the device and to increase the perovskite/HTL interface stability. In this work, we focus on the effect of the interface modifications on the solar cell devices. A detailed discussion about the structural properties of MoS_2 nanosheets and the CsFAMA perovskite layer is presented in the Supporting Information. We found that drop-casting with a colloidal solution of MoS_2 nanosheets results in a decoration of perovskite films by MoS_2 nanosheets. Figures S1−S14 show different characterizations of MoS_2 and DT ligand-modified CsFAMA perovskite films (please see the Supporting Information). Below, we investigate the effect of these surface modifications on the solar cell performance.

2.1. Solar Cell Devices Based on Triple-Cation $Cs_{0.05}(FA_{0.83}MA_{0.17})_{0.95}Pb(I_{0.83}Br_{0.17})_3$ (CsFAMA) Perovskite. Solar cell devices based on CSFAMA perovskite with and without surface modifications with MoS_2 and MoS_2 in combination with DT ligands were compared to investigate how these modifications affect the device performance initially and after aging under dark and light conditions.

Figure 1a−e shows the *JV* measurements of devices with the nomenclatures control, MoS_2, and $DTMoS_2$, as mentioned in Figure S1. The control device has the following layers: FTO/ETL/perovskite/Spiro-OMeTAD/Au, while the MoS_2-treated device has the following layers: FTO/ETL/perovskite/MoS_2 modification/Spiro-OMeTAD/Au configuration, and the $DTMoS_2$-treated device has the following layers: FTO/ETL/perovskite/DT + MoS_2 modification/Spiro-OMeTAD/Au. Figure 1a,c,e depicts the forward−reverse *JV* curves under 1 sun illumination of the fresh devices and Figure 1b,d,f shows the forward−reverse *JV* curves after 2200 h of ageing measurements based on ISOS-D-1 stability protocol.[40] MoS_2- and $DTMoS_2$-treated fresh devices initially show slightly higher efficiency than the control device. They also show slightly higher hysteresis than the control device with nominal values of 1.46, 2.65, and 1.75% for the control device and the modified devices with MoS_2 and $DTMoS_2$, respectively.

All the aged devices after 2200 h show roughly the same amount of hysteresis reduction compared to their fresh counterparts. The devices with MoS_2 and $DTMoS_2$ modification show a higher FF and performance than the control device, although the control device shows low hysteresis of 0.65%. Moreover, the $DTMoS_2$ device shows higher performance compared to the other devices and less hysteresis (1.26%) compared to MoS_2 (1.73%). Table 1 shows the *JV* parameters for the best devices. The results show that the higher performance of the device with $DTMoS_2$ modification is mainly due to an increase of the FF value. Figure S15a shows the *JV* curves of a device fabricated using only DT (1-dodecanethiol) modification of the perovskite film for comparison. The results are similar to the control device, which suggest that the MoS_2 nanosheets are essential to improve the device properties. In Figure S15b, the IPCE and integrated short current density of the fresh cells show roughly the same values indicating that MoS_2 nanosheets and ligand modification do not contribute to the photon-to-electron conversion. Hence, the improvement of the performance of the devices with $DTMoS_2$ and MoS_2 should be sought via interface effects. To examine the stability of the devices, the ISOS-D-1 protocol was performed for 2200 h and then the same devices were used for light cycling measurements based on the ISOS-LC-1 protocol according to the consensus statement for stability assessment.[40]

Table 1. Device Parameters for the Triple-Cation CsFAMA Perovskite-Based Devices

device	PCE (%)	FF (%)	J_{SC} (mA/cm^2)	V_{OC} (V)
$DTMoS_2$	18.90	75.10	22.75	1.11
MoS_2	18.59	74.73	22.78	1.09
Control	18.30	73.15	22.72	1.10

Figure 2a−f shows the comparison of the collected *JV* measurement parameters of the devices extracted during 3100 h. The results show that the devices with $DTMoS_2$ and MoS_2 have enhanced power conversion efficiency (PCE) values compared to the control device, mainly due to retaining the FF. It is worth noticing that the devices with MoS_2 and $DTMoS_2$ do not show any considerable difference in their performance with time. Thus, a more rigorous stability protocol was examined to elucidate the interface modification effects due to the ligand modification in addition to the MoS_2. Light cycling [6 h under simulated 1 sun light-emitting diode (LED) light in an ambient atmosphere and 6 h in dark kept in a N_2 atmosphere] measurement results are indicated in the hatched rectangular box in Figure 2. The *JV* measurements for this part of the experiment were conducted for 900 h, and during this time, measurements were performed after each light exposure for continuous 6 h in ambient air and also after each stabilizing time for 6 h with keeping the devices in dark and under a N_2 atmosphere, which is the protocol ISOS-LC-1.[40] In Figure 2, the device with $DTMoS_2$ shows the least FF degradation and consequently least PCE degradation compared to the other devices, but both the device with $DTMoS_2$ and the device with only MoS_2 have higher device parameters than the control device. Summarizing the stability measurements, the devices with $DTMoS_2$, MoS_2, and the control device have in average retained 92, 91, and 72% of their highest efficiency after 2200 h (ISOS-D-1 protocol) and 80, 75, and 55% after light cycling (ISOS-LC-1 protocol), respectively. To further investigate the stability of the devices, continuous *JV* measurements were performed under simulated sunlight at an ambient temperature and air humidity holding cells at maximum power point (MPP) according to ISOS-L-1.[40]

The MPP tracking for 900 s in Figure S16 revealed the higher stability of the device with $DTMoS_2$ in FF, V_{OC}, and J_{SC} and consequently PCE of the device. It is worthy to point out that the device with MoS_2 also shows higher performance than the control device. The V_{OC} retaining for both MoS_2- and $DTMoS_2$-treated devices besides FF values could be due to charge accumulation inhibition and reducing recombination at the interface of perovskite-HTL,[41,42] and this will be further studied below. Figure 3a demonstrates the overall statistical summary of PCE and FF of the devices. The devices with $DTMoS_2$ and MoS_2 show an obvious narrower range of statistically distributed data indicating higher median, mean, and maximum values compared to the control device. Figure 3b also indicates a clear enhancement of device performance for the $DTMoS_2$-modified device compared to the MoS_2-modified device, summarizing the data collected from ISOS-

https://doi.org/10.1021/acsaem.1c02412
ACS Appl. Energy Mater. 2021, 4, 14080−14092

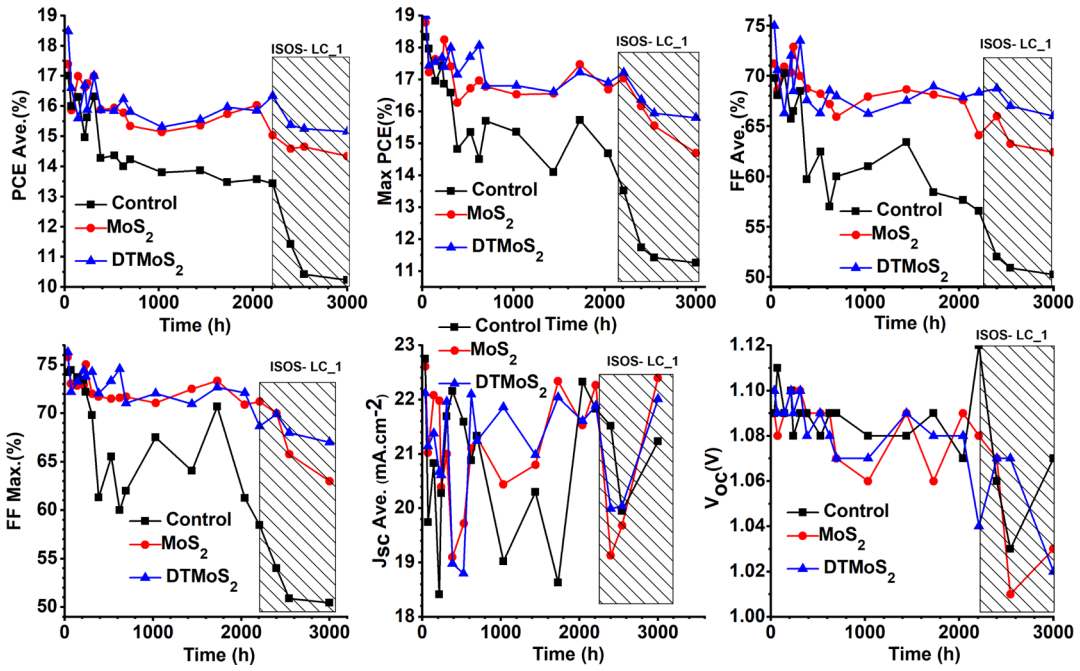

Figure 2. Cell parameters' tracking including (a) PCE average, (b) PCE maximum, (c) FF average, (d) FF maximum, (e) J_{SC} average, and (f) V_{OC} average through the ISOS-D-1 protocol for 2200 h, followed by the ISOS-LC-1 protocol for 900 h (hatched rectangle area) applied to CsFAMA perovskite unencapsulated devices at an ambient atmosphere. ISOS-D-1 is the protocol for stability check, keeping samples in dark and a N_2 atmosphere with sequential measurements at an ambient atmosphere. ISOS-LC-1 is referring to the light cycling protocol in which the device is kept for 6 h under 1 sun simulated LED light in an ambient atmosphere and 6 h kept in dark and under a N_2 atmosphere. Each data point has been obtained by averaging four measurements for each cell and among at least six cells of each category.

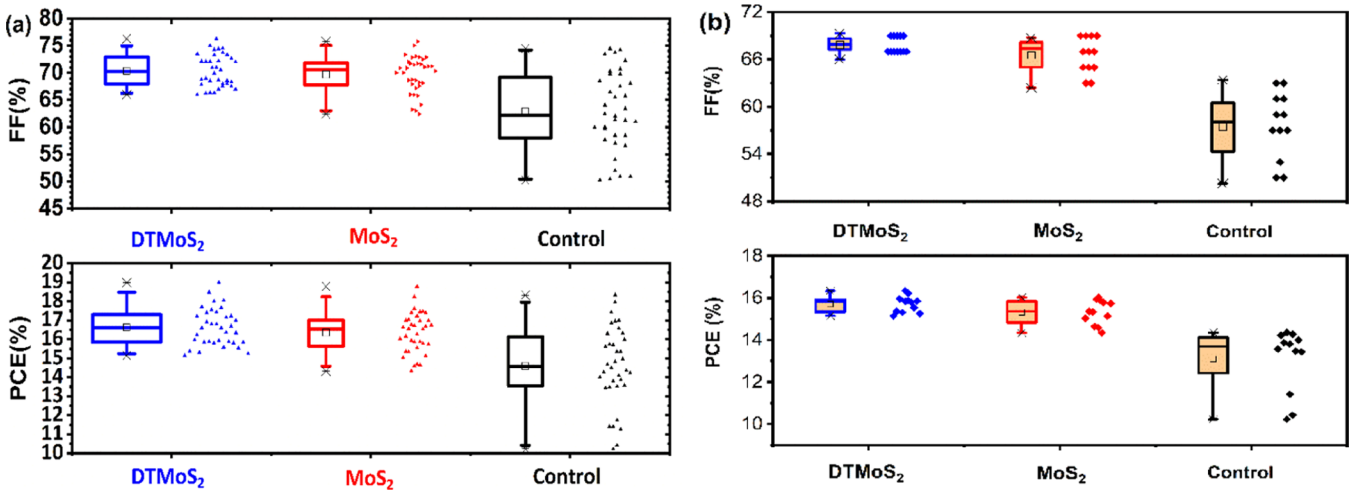

Figure 3. (a) PCE and FF summaries of the cell performance for unencapsulated $DTMoS_2$- and MoS_2-treated CsFAMA perovskite-based devices after ISOS-D-1 or ISOS-LC-1 protocols' tracking, (b) PCE and FF summaries of the cell performance for unencapsulated $DTMoS_2$- and MoS_2-treated CsFAMA perovskite-based devices collected from only ISOS-LC-1 protocol tracking. The whiskers show maximum and minimums in each range of data, the open box square (black) shows the mean value, and the solid color-dependent line shows the median value.

LC-1 protocol tracking time as indicated by a shaded box in Figure 2. This indicates that the $DTMoS_2$ device is more stable under light soaking compared to the device with only MoS_2 modification. Besides stability enhancement, another aspect that is concerned in the perovskite solar cell fabrication especially for the large-scale production purposes is the pinholes and, for example, cracks on the surface of the perovskite which cause short-circuiting. A statistical study of short-circuited cells among all fabricated cells indicates that the number of short-circuited cells has been reduced by roughly 58% due to DT modification and MoS_2 drop-casting on the surface of the perovskite layer. This result suggests that the surface modification reduces the problems with short-circuited cells, which may be important for the large-scale production of perovskite solar cells.

Figure 4a–h demonstrated the PCE, FF, log–log intensity–J_{SC}, and semi log intensity–V_{OC} plots of the fresh cells and the aged cells after 2200 h, respectively. The results confirm the FF enhancement of the devices in the different light intensities, which is related to reduced recombination.[41] Log–log plots of J_{SC} versus light intensity and V_{OC} versus log intensity have been plotted from 10 to 100 mW cm^{-2} to extract the exponent

https://doi.org/10.1021/acsaem.1c02412
ACS Appl. Energy Mater. 2021, 4, 14080–14092

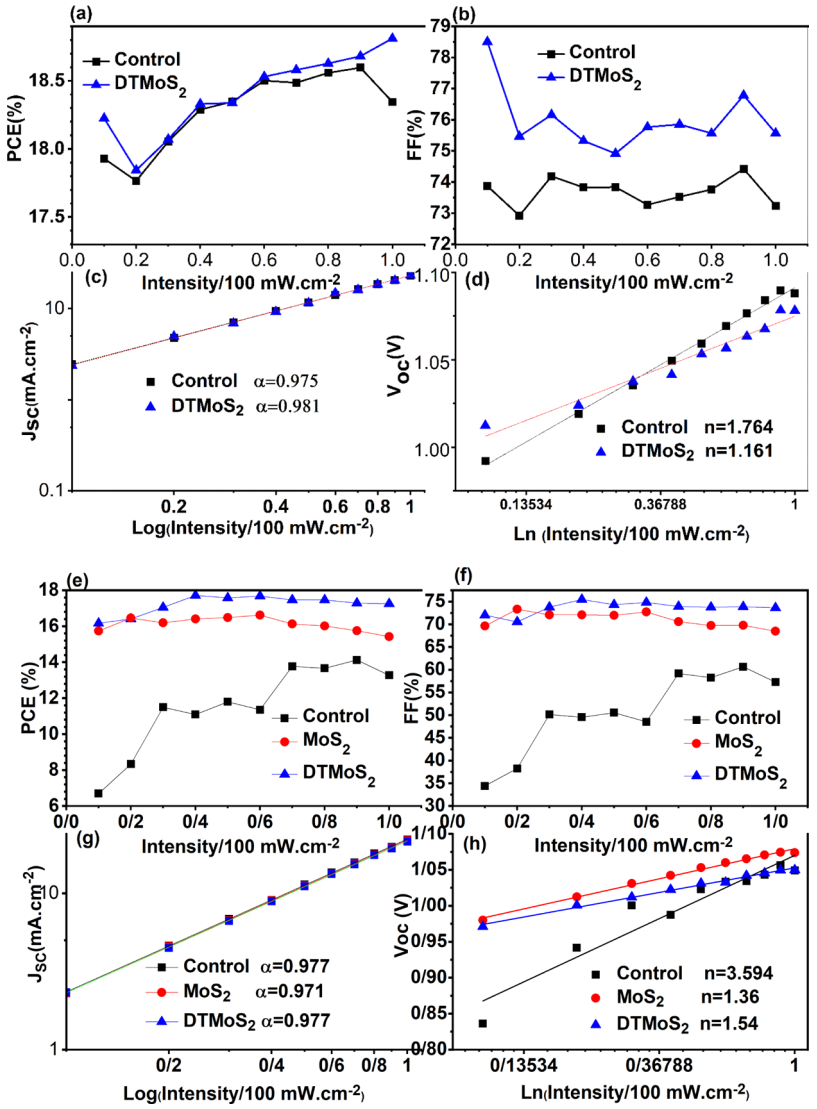

Figure 4. (a) PCE, (b) FF vs sun intensities for fresh cells, (c) log−log J−V plot, and (d) log intensity−V_{oc} plot of the fresh cells CsFAMA perovskite-based nonencapsulated devices, and (e) PCE, (f) FF vs sun intensities for aged (ISOS-D-1) devices, (g) log−log J−V plot, and (h) log intensity−V_{oc} plot of aged devices after 2000 h of tracking of ISOS-D-1 protocol fabricated with CsFAMA perovskite.

α value from $J_{SC} \approx$ (light intensity)$^{\alpha}$[43] and the diode ideality factor (n), respectively.[41,43] The small deviation of α from 1 indicates that the J_{SC} is slightly affected by bimolecular recombination losses which may originate from the bulk or surface defects and quality of the perovskite crystal structure.[43] Generally, for both fresh and aged cells, all devices show high values of $\alpha > 0.97$, and this deviation is the least for the device with $DTMoS_2$. The ideality factor is connected to the extent of trap-assisted recombination losses. The results indicate that the device with $DTMoS_2$ modification has the lowest deviation from the ideal diode, $n = 1$. The ideality factor, n, for the control device has increased from 1.76 to 3.59, while for the device with $DTMoS_2$, it has only increased from 1.16 to 1.54 after aging. A rough estimation of the total trap densities can be obtained by space charge limited current density (SCLC) measurements (see the Supporting Information), and the results are shown in Figure S17a. The calculated trap densities obtained from SCLC measurements which are shown in Figure S17a are 1.95×10^{16}, 1.72×10^{16}, and 1.55×10^{16} 1/cm^3 for the control device and the devices with MoS_2 and $DTMoS_2$, respectively.

To scrutinize more on the trap densities of interfaces due to the application of MoS_2 and DT on the treatment of the perovskite film, Mott−Schottky (MS) plots were extracted from electrochemical impedance spectroscopy (EIS) measurements in dark and in various voltage biases, and the capacitance data were extracted at 10 kHz[44] (see the Supporting Information for MS calculation details). MS plots are shown in Figure S17b, N, and the obtained trap densities for aged devices (2200 h) at the interface of ETL/perovskite or perovskite/HTL are 0.76×10^{16}, 0.51×10^{16}, and 0.38×10^{16} 1/cm^3 for the control device and the devices with MoS_2 and $DTMoS_2$, respectively. In analogy with SCLC analyses, the devices with $DTMoS_2$ and MoS_2 modifications show less trap densities than the control device. It is worth mentioning that the ratios of n_{trap} calculated from SCLC measurements for $n_{trap}^{DTMoS2}/n_{trap}^{control}$ is equal to 0.9, while this ratio from MS analyses is 0.5. This difference can be interpreted as follows: in SCLC measurement under the static conditions, both bulk and interface recombination mechanisms are involved in filling trap states, while in MS analysis, due to the choice of frequency at 10 kHz, the dominant recombination mechanism is the

https://doi.org/10.1021/acsaem.1c02412
ACS Appl. Energy Mater. 2021, 4, 14080−14092

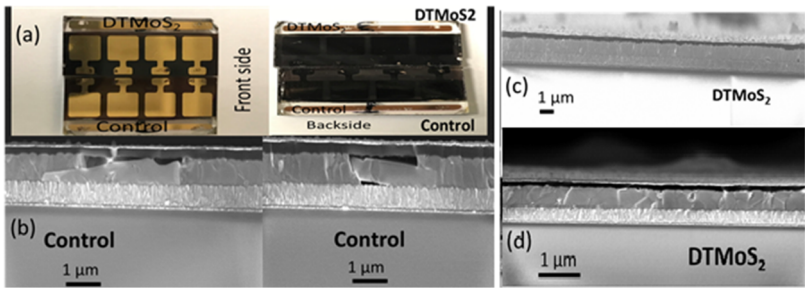

Figure 5. (a) Front-backside photographs of the control device and $DtMoS_2$-modified device, (b) two different corresponding cross SEM images of the control CsFAMA perovskite-based device, and (c,d) corresponding cross SEM images of the device modified with $DTMoS_2$. The cross SEM images were prepared after ISOS-D-1 and ISOS-LC-1 protocol measurements of unencapsulated devices.

interface recombination.[42,44] Hence, the results suggest that DT and MoS_2 modifications reduce the trap states at the interface of perovskite/HTL.[41,44,45]

The flat band potential, V_{bi}, was calculated from the intercept of linear fitting from MS analysis to 1.07, 1.03, and 1.05 V for the control device and the devices with MoS_2 and $DTMoS_2$, respectively. Similar values were therefore obtained, although the incorporation of MoS_2 nanosheets with a different Fermi level compared to the perovskite and HTL may be expected to affect the band-alignment.[46] To investigate the effect of MoS_2 and DT on the energy levels of the resultant device in more detail, the work functions of the control device and the device with $DTMoS_2$ were measured using Kelvin probe and compared under dark and light conditions in Figure S18.

It should be noticed that the Kelvin probe measurement was performed by a gold tip of width 600 nm, so the work function measured is not a local but average value because over 600 nm × 600 nm area, the probe would interact with large numbers of MoS_2 crumpled nanosheets. Thus, the Kelvin probe measurements present the average work function of that surface area. The results show a significant difference between the bare perovskite film and $DTMoS_2$-modified film, and the average work function values of −5.02 and −4.67 eV with respect to vacuum are obtained for the CsFAMA perovskite and $DTMoS_2$-modified CsFAMA perovskite, respectively.[47] A rough estimation of the valence band position of bare CsFAMA perovskite film and $DTMoS_2$-modified perovskite film can be obtained from the Kelvin probe measurements in combination with the band gap of the perovskite from the light absorption spectrum (the perovskite band gap is calculated to 1.65 eV). Assuming the perovskite is close to intrinsic, with a low number of defects, the Fermi level is expected to be close to the middle of the band gap, and we can estimate the valence band position to be −5.8 and −5.5 eV for the bare CsFAMA perovskite film and $DTMoS_2$-modified perovskite film, respectively. With respect to the HTL valence band (−5.2 eV),[47] the hole transfer would be more facile and efficient due to the change of the valence band position of the perovskite with $DTMoS_2$.

To investigate the recombination in MoS_2- and $DTMoS_2$-modified devices, square-wave modulated transient photovoltage decay under different light intensities were measured at the frequency of 2 Hz. The data henceforth were extrapolated by a biexponential decay function according to the previous reports.[48,49] The results that are depicted in Figure S19 indicate the increase of both time constants (τ_1, τ_2)[49] for the devices with $DTMoS_2$ and MoS_2. The results agree with SCLC and MS analyses, which also suggested the decrease of interface states and therefore reduced recombination for the devices with $DTMoS_2$ and MoS_2. Chen et al. have concluded that the recombination processes are due to two major phenomena. One is the free electron−hole recombination with a faster time scale and the other one is the ion trapping—charge recombination which is mostly considered I^- and holes in their report.[49] Nyquist plots of the samples have been plotted in Figure S20a−d. The results may indicate ion migration hindrance at the interface of perovskite/HTL by reduction or elimination of negative capacitance for the devices with MoS_2 and $DTMoS_2$ according to the report of Ebadi et al.[50,51]

It can be inferred from Figure S20c,d that the control sample suffers from the negative capacitance in dark measurement kept at V_{OC} which is not the case for the device modified with $DTMoS_2$. Figure S20e demonstrates the induced negative loop for the control device after stability examination according to the ISOS-LC-1 protocol,[40] while the other samples do not show any negative capacitance and their inductive loop is not pronounced at the same low frequencies. According to Ebadi et al.[51] and Ghahremanirad et al.,[52] this negative capacitance cannot be directly interpreted as the ion or charge accumulation at the interfaces but they rather state that a transient current there exists upon slow ion displacement. However, the high capacitive behavior in low frequencies could be attributed to modified charge injection processes. This phenomenon according to Chen et al.[49] has been mostly attributed to ion-free carrier recombination for that they used a Warburg element or Gerischer element in their simulations.[49] Therefore, they have attributed the time constant obtained in dark and under bias-voltage to electron−hole recombination, while they believe the time constant obtained under sunlight measurement is related to the ion-carrier recombination.[49] The comparison of Nyquist plots in dark and at zero bias-voltage for the control device and the device with $DTMoS_2$ shows high shunt resistance for the device with $DTMoS_2$ according to Albadri et al.[53] The semicircle resistance in dark and zero bias-voltage if perturbed by small voltage variation (20 mV) can be interpreted as the shunt resistance.[43] Moreover, a rough estimation of the fast recombination process can be expressed as $\tau_{fast} = 1/\omega|\max(\mathrm{Im}(-Z))$[51] or can be extracted from the log−log plot Bode plot of $\mathrm{Im}(-Z)$. It is plotted for three samples in Figure S21 measured at 1 sun and V = 0 V. The results obtained 0.50×10^{-4}, 0.61×10^{-4}, and 0.99×10^{-4} s for the control device and devices with MoS_2 and $DTMoS_2$, respectively, which is in excellent agreement with photovoltage decay measurements for simulated 1 sun (Figure S20-inset) which are 0.48×10^{-4}, 0.56×10^{-4}, and 1.04×10^{-4} s, respectively. Chen et al. has attributed this time constant

https://doi.org/10.1021/acsaem.1c02412
ACS Appl. Energy Mater. 2021, 4, 14080−14092

mostly due to the recombination of free carriers and other species (ions movement) in the perovskite solar cells.[49] It should be noticed that the low impedance value of samples under sunlight and biased voltages in the low-frequency region is not related to the charge accumulation according to Ebadi et al[51] Moreover, the same trend in the high-frequency region is simply related to the increase of conductivity of the device.[51] Hence, it can be conveyed that the application of DT and MoS_2 on the modification of the interface may also have some effects on ion interaction and migration from perovskite to HTL and vice versa.

To further investigate the stability enhancement of the devices, the photographs and their corresponding SEM cross-sectional images of the unencapsulated device with $DTMoS_2$ and the control device are presented in Figure 5a−d. These images have been taken from the unencapsulated devices after ISOS-D-1 and ISOS-LC-1 protocols' tracking in an ambient atmosphere and humidity (20−25%). However, on this scale, we do not observe any significant differences. A more detailed analysis on a smaller length scale or using other techniques to specifically address changes at the interface is necessary. We therefore instead below study the interfaces in more detail using EIS.

2.2. Interface Studies Using EIS Measurements. Chen et al. has studied the EIS of perovskite solar cells in (V, I) space in which they mapped the EIS of cells by a fixed biased voltage and in different light intensities and then in a fixed intensity with different applied bias-voltages to the cells.[49] Based on their reports, the corresponding lifetime for electron−hole recombination (τ_{HF}) is determined by considering both the lifetime extracted from the dark condition and at open-circuit voltage (τ_{dark}) and under 1 sun and with zero bias-voltage (τ_{light}).[49] Then, they are related with the following relation

$$\frac{1}{\tau_{HF}} = \frac{1}{\tau_{light}} + \frac{1}{\tau_{dark}} \quad (1)$$

where τ_{HF} denotes the relaxation time of free carriers in the high-frequency region in the simulated circuit and is calculated directly from τ = RC of the high-frequency part of the circuit. Figure S22 shows the fitted curves and Figure S23 depicts their corresponding simulated circuits for the dark condition, V = V_{OC} and under 1 sun intensity and V = 0 V. We have used ZW (Warburg) element and ZG (Gerischer) element in the simulation, while ZW means that ions first move in the perovskite bulk to the interfaces then recombine with free carriers at the interfaces and ZG means that ion movement is accompanied by continuous free carrier recombination.[49] The result of τ_{HF} calculations obtained values of 3.303, 2.706, and 0.356 μs for the modified $DTMoS_2$ and MoS_2 CsFAMA devices and the control CsFAMA device, respectively. This indicates, higher free carriers' lifetime in agreement with the photovoltage decay measurements. To further discuss this improvement of charge lifetime in MoS_2-treated devices, one has to bear in mind that the increase of charge lifetime in low-frequency modulated photovoltage measurements is attributed to the ion movements at the interfaces.[53] The presence of DT ligand and MoS_2 nanosheets at the interface of perovskite/HTL has reduced the trap recombination as it has also been reported for interface passivation of quadruple-cation solar cells by Albadri et al.[53]

Many reports have tried to relate the hysteresis of perovskite solar cells to ion migration and charge accumulation,[42] although Calado et al.[45] have reported that ion migration exists even in perovskite with minimal hysteresis. On the other hand, a broad consensus has been made that hysteresis is due to mobile ions.[54] Recently, it has been suggested that slow ion migration and its relevant screening field is not responsible for the hysteresis, but instead, the formation and release of interfacial charges are the dominant reason.[42] Surprisingly, they have found a time-dependent ion concentration related to the chemical binding of iodide with Spiro-OMeTAD at the interface of perovskite/HTL.[42] We emphasize that upon deposition of MoS_2 interfacial trap passivation results in enhancement of the device performance,[55] and an increase in the hysteresis about 0.6% compared to the control device is also observable. To explain this phenomenon, we must refer to the dielectric constant difference between perovskite (47.5)[56] and MoS_2 nanosheets (4 for E = 1.2 V/450 nm < 0.01 V/Å),[57] and high capability of surface polarization of MoS_2 nanosheets at their basal planes.[57] According to Weber et al.,[42] iodine ion accumulation on the interface of perovskite/HTL can lead to an electric field in the opposite direction of external electric field and can polarize the surface of MoS_2 nanosheets locating at the interface with the opposite charge leading to an internal electric field right at the interface. The JV measurements are indicating a small decrease of 10−20 mV in V_{OC} in repetitive measurements of devices with $DTMoS_2$ and MoS_2, but after the device relaxation, the original values are recovered. It was also observed that due to ligand modification, $DTMoS_2$ devices showed slightly higher V_{OC}, and less hysteresis compare to the device with MoS_2. This can be due to better band alignment, less polarizability of MoS_2 at the interface, and better anchoring to the perovskite surface. Another possible scenario for hysteresis increase with superiority of performance for MoS_2-treated devices can be due to the time-dependent ion accumulation (within few ms according to Weber et al.[42]) at the interface of perovskite/$DTMoS_2$ (MoS_2)/HTL, and there is a built-in electric field at both sides of MoS_2 nanosheets that causes an increase in the potential barrier for hole injection and results in an induced hysteresis according to Ebadi et al.[51] Moreover, due to the well passivation of traps at the interface at the same time, it not only does not affect the performance of the device but also enhances its stability.[58]

Klotz[59] has discussed both inductive hook and negative loop (capacitance) as follows: if the ion migration in the direction of voltage positively contributes to the performance of the electrode, a negative low-frequency hook or inductive loop will appear, but if the ion migration in the direction of voltage causes the driving forces destructively contribute in the electrode performance, there will be an additional negative semicircle to that. Based on this, our results suggest that the application of DT and MoS_2 at the interface of perovskite/HTL suppresses the negative effects of ion migration. In a parallel interpretation, Ebadi et al.[51] have discussed that how ion pileup on the negative electrode can result in the reduction of the potential barrier for the electrons and results in hysteresis in the forward scans as well as negative capacitance usually observed for SnO_2-based ETL devices.[51] They have also emphasized the effect of Bi doping as induction of trap states at the interface and lowering the resultant work function and built-in potential that causes an apparent negative capacitance.[51] In analogy with that, we state that our method of perovskite surface passivation with MoS_2 nanosheets and DT has resulted in the removal of observed negative capacitance. In addition to that, we can also emphasize that

https://doi.org/10.1021/acsaem.1c02412
ACS Appl. Energy Mater. 2021, 4, 14080−14092

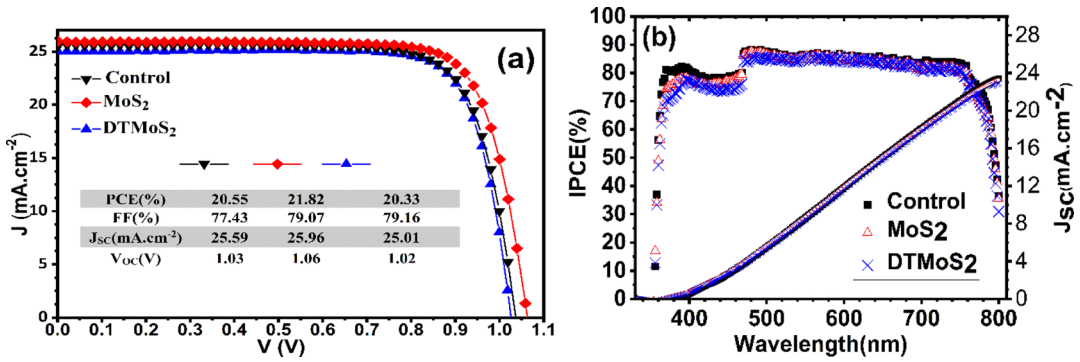

Figure 6. (a) Reverse scan $J-V$ measurements of the two-step FAMA-Cl perovskite-based devices, and (b) IPCE and integrated short current density of the corresponding cells.

the local work function increases for $DTMoS_2$ devices and decreases the hole recombination probability as well.

2.3. Solar Cell Devices Based on Two-Step Preparation of the FAMA-Cl Perovskite Film. The results above were obtained for a CsFAMA triple-cation perovskite deposited in a single step by the antisolvent injection technique. However, it is also interesting to investigate if the MoS_2 interface modification also improves other types of perovskite solar cell devices. We have therefore also investigated the effect of the perovskite interface modifications on a different type of perovskite abbreviated as FAMA-Cl perovskite prepared using a two-step method (please see the Supporting Information for the preparation details).

This type of perovskite has been prepared with a two-step method with no antisolvent involved. The *JV* curves of the champion devices with FAMA-Cl perovskite are shown in Figure 6a. The devices with MoS_2 and $DTMoS_2$ modifications show higher efficiencies compared to the control device, which is mainly due to a higher FF (Table 2). Figure 6b shows the IPCE of the samples and their correspondence integrated current density, and MoS_2 and DT are not contributing in the photon-to-current conversion efficiency, so any enhancement in the performance of solar cells might be attributed to the interface modification. To study the stability of the fabricated devices, the ISOS-D-1 protocol was performed and the statistical analyses of the cell parameters have been summed up in Figure 7a–k. Although all devices show high performance in 1700 h of tracking, detailed analysis on PCE maximum, minimum, and average as well as FF maximum, minimum, and average values, and J_{SC} maximum and average, and V_{OC} average values were performed to find which factor is the most influenced due to MoS_2 and DT modification. The data were collected for each point by averaging six repetitions of measurements for each cell among at-least nine cells in each category.

Table 2. Device Parameters for the FAMA-Cl Two-Step High-Efficiency Perovskite-Based Devices

device	PCE (%)	FF (%)	J_{SC} (mA/cm^2)	V_{OC} (V)
MoS_2	21.80	79.55	25.97	1.04
$DTMoS_2$	20.33	79.16	25.02	1.02
control	20.55	77.43	25.60	1.03

The results show that the PCE of the device with MoS_2 remains above 20%, from 3 days after the cell fabrication. The device with $DTMoS_2$ modification also kept higher average and maximum PCE values than the control device. The MoS_2-modified device reached a PCE of 21.8% and a FF of 81%, while the $DTMoS_2$-modified device obtained a PCE of 20.33% and a FF of 79.5%. The statistical summaries of PCE and FF values of the devices are shown in Figure 8. The results suggest that the devices with MoS_2 and $DTMoS_2$ modifications have higher performance and stability compared to the control device, similar to what we observed for the CsFAMA perovskite devices.

To further check the stability of the devices, MPP tracking was performed on the unencapsulated second type of devices for 900 s, and the results are shown in Figure S24. These results show that the devices with MoS_2 and $DTMoS_2$ modifications are more stable than the control devices in all the parameters. The cell parameters were measured under different simulated sunlight intensities and are displayed in Figure S24. The PCE and FF values of the devices with MoS_2 and $DTMoS_2$ modification are frequently higher than the control device, as shown also in Figure 8 for the champion devices fabricated by FAMA-Cl perovskite.

The ideality factor (n) of the devices was extracted from the log intensity–V_{OC} plot, as depicted in Figure S25. It shows that the device with MoS_2 modification has the least deviation from ideal diode behavior compared to the other devices. To investigate the effect of trap state densities, SCLC measurements were performed for fresh devices and after 1440 h of ISOS-D-1 tracking, and the results are shown in Figure S26a. Besides the trap density values, the change in their measurement due to the aging process can be related to the interface effect of MoS_2.

The values obtained from Figure S26a are 0.99×10^{16} and 1.16×10^{16} 1/cm^3 for fresh and aged devices with MoS_2 modification, while they are 1.49×10^{16} and 1.78×10^{16} 1/cm^3 for the fresh and aged control device, respectively. It is also inferred that the change of trap density is higher for the control device compared to the device with MoS_2 modification.

MS analysis was also performed complimentarily, and the results are depicted in Figure S26b (left axis) included with the capacitance of the devices (right axis). The trap densities obtained from the slope of the linear fit of the depletion layer are 0.96×10^{16} and 0.39×10^{16} for the control and MoS_2-modified devices, respectively. Similarly, as already observed for the case of CsFAMA solar cells, the application of MoS_2 has had a significant effect on the interface of this type of perovskite due to the significant decrease in trap densities.

To investigate this effect in more detail, photovoltage decay measurements were performed in different light intensities and

https://doi.org/10.1021/acsaem.1c02412
ACS Appl. Energy Mater. 2021, 4, 14080–14092

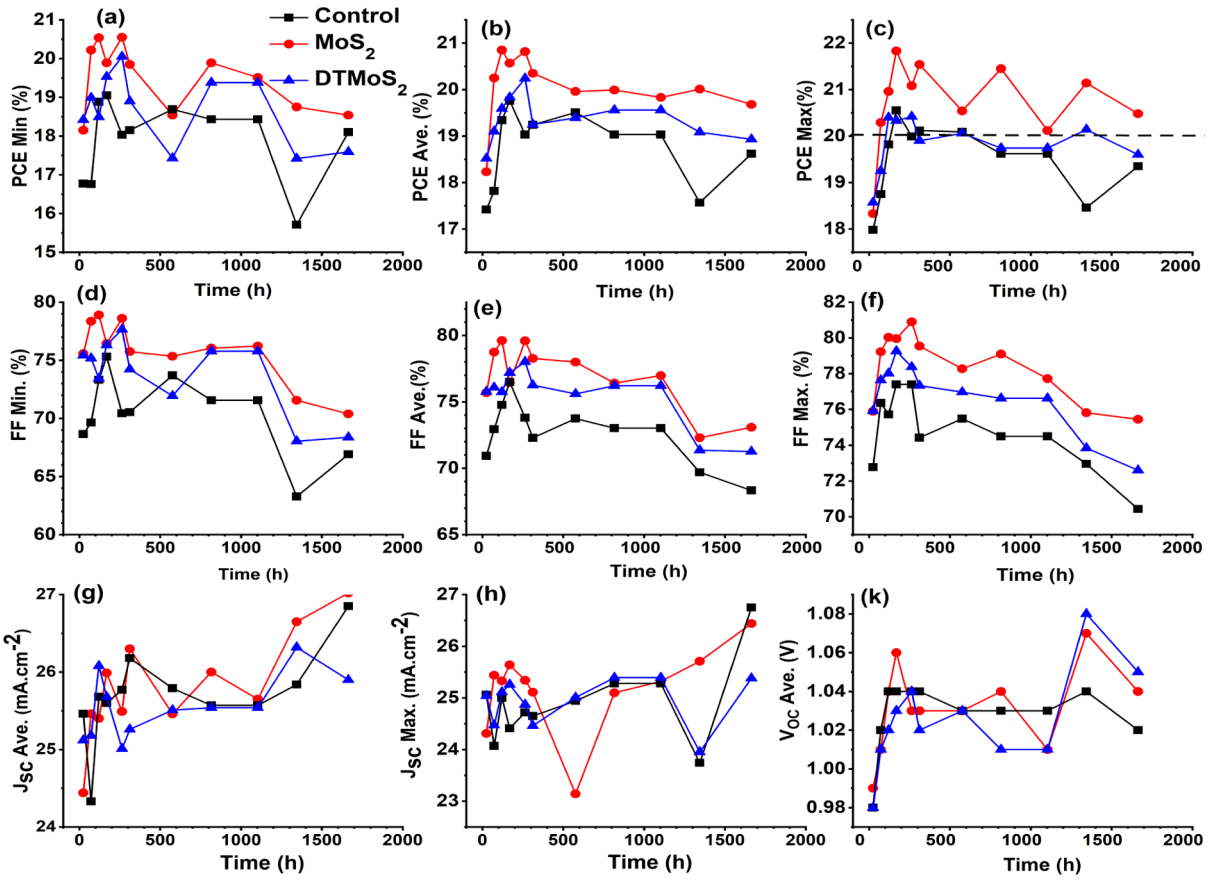

Figure 7. Cell parameters' tracking including (a) PCE minimum, (b) PCE average, (c) PCE maximum, (d) FF minimum, (e) FF average, (f) FF maximum, (g) J_{SC} average, (h) J_{SC} average, and (k) V_{OC} average utilizing performing ISOS-D-1 protocol for FAMA-Cl two-step perovskite-based unencapsulated devices at an ambient atmosphere. Each value has been obtained by averaging five repetitions of measurements for each cell among at least nine cells in each category.

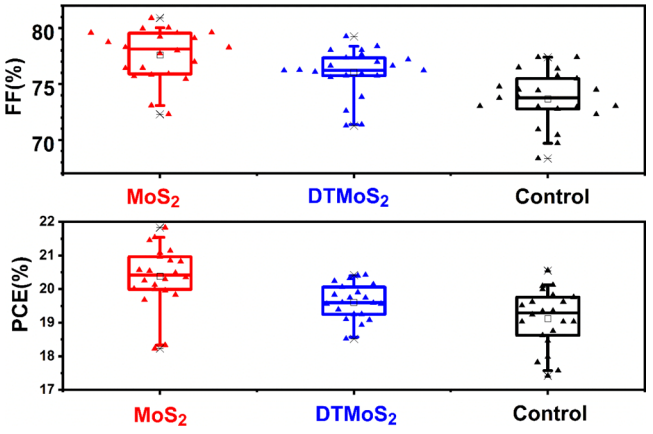

Figure 8. Summary of PCE and FF of the control and MoS_2- and $DTMoS_2$-treated devices prepared using the two-step FAMA-Cl perovskite deposition.

the extracted lifetime from a biexponential function fitting are plotted in Figure S27. MoS_2- and $DTMoS_2$-modified devices show significant improvement in the calculated lifetime compared to the control device. It is worth noticing that the device with $DTMoS_2$ has the highest value in both time-constants[53] in good agreement with the results of the triple-cation case. Figure S28 depicts the Nyquist plots of the devices in different bias-voltages under 1 sun, and dark held at V_{OC}. As it has been already discussed by Chen et al.,[49] the impedance data in low frequencies (less than 300 Hz) is attributed to the mechanism of ion migrations inside the device.[50,51] As it can be seen, for the control device, the low-frequency Nyquist plots at different voltages show more scattered behavior and negative capacitance which are not observed for the devices with MoS_2 and $DTMoS_2$ modification. The comparison of three devices under 1 sun and biased at V_{OC} in Figure S28 show higher impedance with a clear inductive loop touching the zero line, indicating very high resistance in the ion transfer mechanism for the control sample, while the devices with $DTMoS_2$ and MoS_2 modifications demonstrate a diffusive behavior in low frequencies.

Moreover, comparison of Nyquist plots of the control device, the devices with MoS_2 and $DTMoS_2$ modifications in Figures S20a–d and S28, for CsFAMA perovskite and FAMA-Cl perovskite, respectively, shows compatible results. Both of the figures suggest an enhancement of charge extraction and decrease of resistance by imposing either light intensity or forward bias. The former increases the number of photo-generated carriers and consequently the chemical capacitance, and the latter one is due to shifting the Fermi level toward the conduction band of SnO_2 and faster charge extraction as it is stated elsewhere.[60] Another major aspect for both types of perovskites in their corresponding Nyquist plots is that the control devices for both cases (Figures S20 and S28) in the low-frequency regime (ion migration regime) do not show a consistent pattern, while the devices with MoS_2 and $DTMoS_2$ show almost a linear diffusive behavior. The most interesting

https://doi.org/10.1021/acsaem.1c02412
ACS Appl. Energy Mater. 2021, 4, 14080−14092

aspect that is observed from Nyquist plots for the two types of perovskites at complete chronology in both Figures S20 and S28 is the trend of decrease of resistance between the three devices which is $R_{control} > R_{MoS2} > R_{DTMoS2}$. The reason behind this fact is suggested that under 1 sun illumination and bias application, the number of photogenerated carriers increases significantly, resulting in the increase of the chemical capacitance. On the other hand, Wang suggested that the device with a higher hole extraction rate at the interface of perovskite/HTL own a lower charge accumulation at the interface of ETL/perovskite.[60] Hence, it results in the decrease of the chemical capacitance of the device and also the impedance resistance, in analogy with the MS analyses. Thus, EIS analyses for both types of perovskites indicate that with MoS_2 and $DTMoS_2$ modifications, hole extraction at the interface of perovskite/HTL may be improved and can result in less charge accumulation.[60]

3. CONCLUSIONS

In this work, MoS_2 nanosheets were introduced as an interface modifier in perovskite solar cells between the perovskite and the HTL. The effects on efficiency and stability were investigated and it was found that both efficiency and stability are enhanced by this interface modification. Both double-cation (FAMA-Cl) and triple-cation (CSFAMA) perovskites were investigated together with this interface modification, and we also investigated the effect of DT as bridging ligand modification of the perovskite surface before depositing the MoS_2 nanosheets. Different methods were used to understand how the interface modification affects the perovskite solar cell and why the solar cell performance and stability are enhanced. From the results, we suggest that the interface modifications reduce the recombination at the perovskite/HTL interface, improve hole transport from the perovskite to the HTL, and reduce ion movement at the interface. This type of interface modification, therefore, has several positive effects on the perovskite solar cell device and maybe an important step for increasing efficiency together with the stability of the perovskite solar cell devices.

4. EXPERIMENTAL SECTION

Synthesis of MoS_2 nanosheets and preparation of its dispersion solution, perovskite, and doped Spiro-OMeTAD solutions' preparation, and the characterization methods are described in detail in the Supporting Information.

4.1. Device Fabrication. *4.1.1. Substrate Cleaning.* Standard conductive FTO glasses (TEC 15, Pilkington) were cut in twin slides of 2.4 cm × 1.4 cm, and subsequently, 3 mm of one side was etched using zinc powder and HCl 2 M solution for 5 min. Then, the substrates were cleaned and washed using bath sonication in three subsequent steps by water with 2% volume RBS 50 (Sigma-Aldrich), acetone, and isopropanol (97%) of Merck Co. each for 30 min, respectively. Then, the substrates were dried using N_2 gas blowing, followed by masking 3 mm of the nonetched side for SnO_2 nanoparticle deposition as ETL.

4.1.2. ETL Deposition. The SnO_2 nanoparticle colloidal solution was obtained from ALFA AESAR Company [tin(IV) oxide, 15% in H_2O colloidal dispersion]. A diluted solution of water/SnO_2 nanoparticles' solution with a volume ratio of 4:1, respectively, was prepared. The substrates were UV−ozone cleaned for 25 min. 0.4 mL of the colloidal solution was spun on UV−ozone cleaned substrates with 3000 rpm and a ramp-up of 3000 rpm/s for 30 s, and then, the substrates were placed on a hotplate preheated at 150 °C for 1 h.

4.1.3. Triple-Cation CsFAMA Perovskite Deposition. The deposition of perovskite layer, MoS_2 drop-casting, and HTL deposition were performed in a N_2 filled glovebox with controlled humidity and temperature.

Perovskite solution (130 μL) was dropped on the precleaned ETL-deposited substrates (2.4 × 2.8 cm) by O_3 which was for 30 min and subjected to a two-step spin-coating protocol. The first step was at 1000 rpm with an acceleration of 200 rpm/s for 10 s and the second step was at 6000 rpm with an acceleration of 2000 rpm/s for 20 s. In the last 5 s of the second step, chlorobenzene (190 μL) was injected to wash out the solvent and the film turned dark-brown quickly. Then, the substrates were placed immediately on the adjusted hot plate to 100 °C and were kept for 1 h.

4.1.4. FAMA-Cl Perovskite Solution Deposition for Obtaining High-Efficiency Cells (PCE > 20%). 1.5 M PbI_2 was dissolved in a mixture of dimethylformamide and dimethyl sulfoxide (9:1 volume ratio) and then stirred at 70 °C overnight. Prepared PbI_2 solution was coated on the SnO_2 layer at 1500 rpm for 20 s and 5000 rpm for 30 s. Mixed cation halide solution [FAI (90 mg), MAI (6.5 mg), and MACl (9 mg) mixed in isopropanol (1 mL)] was spin-coated on the PbI_2 layer at 2000 rpm for 30 s. After finishing the spin-coating, the perovskite film was taken out to ambient air and annealed at 145 °C for 25 min. This type of perovskite is named "FAMA-Cl" for discrepancy purposes in the main text.

4.1.5. MoS_2 Deposition and Ligand-Modified MoS_2 Deposition on Perovskite Films. After cooling of shiny perovskite films, the prepared colloidal solution of MoS_2 nanosheets was drop-cast in two sequential steps (optimized condition). For each step, MoS_2 colloidal (0.5 mg/mL, 100 μL) was drop-cast while spinning at 3000 rpm for 20 s. To make sure of isopropanol evaporation, 3 min of time interval was considered between these two sequential drop-casting processes.

For ligand modification of perovskite and deposition of MoS_2 nanosheets, a solution containing DT [$CH_3(CH_2)_{10}CH_2SH$: Adrich] in isopropanol anhydrous (12 μL in 2 mL) was employed. 250 μL of this solution was spread on the perovskite film for 1 min to functionalize the surface and then spin-coated at 3000 rpm with a ramp of 1500 rpm/s for 30 s immediately after its deposition, and two subsequent MoS_2 solution drop-casting processes were performed as explained above.

4.1.6. HTL Deposition. The doped-Spiro-OMeTAD solution (50 μL) was injected while the film (modified perovskite and bare perovskite) was spinning at 4000 rpm for 24 s with a ramp-up 4000 rpm/s.

4.1.7. Electrode Deposition. 80 nm of gold was deposited using a physical vapor deposition instrument with the following protocol: 5 nm was deposited with the rate of <0.01 nm/s, then from 5 to 10 nm, the rate was 0.01 nm/s, and from 10 to 80 nm, the rate was 0.08 nm/s.

■ ASSOCIATED CONTENT

Supporting Information

The Supporting Information is available free of charge at https://pubs.acs.org/doi/10.1021/acsaem.1c02412.

MoS_2 synthesis and solution preparation for device fabrication; experimental characterizations and analysis of MoS_2 nanosheets, perovskite thin films, and devices; and SCLC and MS analyses (PDF)

■ AUTHOR INFORMATION

Corresponding Authors

Masoud Karimipour − *Department of Chemistry-Ångström, Physical Chemistry, Uppsala University, Uppsala 75120, Sweden; Department of Physics, Faculty of Science, Vali-e-Asr University of Rafsanjan, Rafsanjan 77139-36417, Iran;* orcid.org/0000-0002-6619-4798; Email: Masoud.karimipour@gmail.com

Erik M. J. Johansson − *Department of Chemistry-Ångström, Physical Chemistry, Uppsala University, Uppsala 75120,*

https://doi.org/10.1021/acsaem.1c02412
ACS Appl. Energy Mater. 2021, 4, 14080−14092

Sweden; orcid.org/0000-0001-9358-8277;
Email: erik.johansson@kemi.uu.se

Authors

Sepideh Khazraei − *Department of Chemistry-Ångström, Physical Chemistry, Uppsala University, Uppsala 75120, Sweden*

Byeong Jo Kim − *Department of Chemistry-Ångström, Physical Chemistry, Uppsala University, Uppsala 75120, Sweden*

Gerrit Boschloo − *Department of Chemistry-Ångström, Physical Chemistry, Uppsala University, Uppsala 75120, Sweden*; orcid.org/0000-0002-8249-1469

Complete contact information is available at: https://pubs.acs.org/10.1021/acsaem.1c02412

Author Contributions

The manuscript was written through contributions of all authors. All authors have given approval to the final version of the manuscript.

Notes

The authors declare no competing financial interest.

■ ACKNOWLEDGMENTS

The authors acknowledge the financial support obtained from the Swedish Energy Agency, Olle Engkvist Foundation, and ÅForsk. M.K. would like to thank Amin Kaveh, Ph.D. student from the IT department, Uppsala University, for writing the R-studio code for the statistical data analysis.

■ REFERENCES

(1) Saliba, M.; Matsui, T.; Seo, J.-Y.; Domanski, K.; Correa-Baena, J.-P.; Nazeeruddin, M. K.; Zakeeruddin, S. M.; Tress, W.; Abate, A.; Hagfeldt, A.; Grätzel, M. Cesium-Containing Triple Cation Perovskite Solar Cells: Improved Stability, Reproducibility and High Efficiency. *Energy Environ. Sci.* **2016**, *9*, 1989−1997.

(2) Zhou, H.; Chen, Q.; Li, G.; Luo, S.; Song, T.-b.; Duan, H.-S.; Hong, Z.; You, J.; Liu, Y.; Yang, Y. Interface Engineering of Highly Efficient Perovskite Solar Cells. *Science* **2014**, *345*, 542−546.

(3) Mei, A.; Li, X.; Liu, L.; Ku, Z.; Liu, T.; Rong, Y.; Xu, M.; Hu, M.; Chen, J.; Yang, Y.; Grätzel, M.; Han, H. A Hole-Conductor−Free, Fully Printable Mesoscopic Perovskite Solar Cell with High Stability. *Science* **2014**, *345*, 295−298.

(4) Yang, W. S.; Noh, J. H.; Jeon, N. J.; Kim, Y. C.; Ryu, S.; Seo, J.; Seok, S. I. High-Performance Photovoltaic Perovskite Layers Fabricated through Intramolecular Exchange. *Science* **2015**, *348*, 1234−1237.

(5) Ke, W.; Fang, G.; Liu, Q.; Xiong, L.; Qin, P.; Tao, H.; Wang, J.; Lei, H.; Li, B.; Wan, J.; Yang, G.; Yan, Y. Low-Temperature Solution-Processed Tin Oxide as an Alternative Electron Transporting Layer for Efficient Perovskite Solar Cells. *J. Am. Chem. Soc.* **2015**, *137*, 6730−6733.

(6) Momblona, C.; Gil-Escrig, L.; Bandiello, E.; Hutter, E. M.; Sessolo, M.; Lederer, K.; Blochwitz-Nimoth, J.; Bolink, H. J. Efficient Vacuum Deposited Pin and Nip Perovskite Solar Cells Employing Doped Charge Transport Layers. *Energy Environ. Sci.* **2016**, *9*, 3456−3463.

(7) Hu, Q.; Wu, J.; Jiang, C.; Liu, T.; Que, X.; Zhu, R.; Gong, Q. Engineering of Electron-Selective Contact for Perovskite Solar Cells with Efficiency Exceeding 15. *ACS Nano* **2014**, *8*, 10161−10167.

(8) Nie, W.; Tsai, H.; Asadpour, R.; Blancon, J.-C.; Neukirch, A. J.; Gupta, G.; Crochet, J. J.; Chhowalla, M.; Tretiak, S.; Alam, M. A.; Wang, H.-L.; Mohite, A. D. High-Efficiency Solution-Processed Perovskite Solar Cells with Millimeter-Scale Grains. *Science* **2015**, *347*, 522−525.

(9) Park, J. H.; Seo, J.; Park, S.; Shin, S. S.; Kim, Y. C.; Jeon, N. J.; Shin, H.-W.; Ahn, T. K.; Noh, J. H.; Yoon, S. C.; Hwang, C. S.; Seok, S. I. Efficient CH3NH3PbI3 Perovskite Solar Cells Employing Nanostructured P-type NiO Electrode Formed by a Pulsed Laser Deposition. *Adv. Mater.* **2015**, *27*, 4013−4019.

(10) Yi, C.; Luo, J.; Meloni, S.; Boziki, A.; Ashari-Astani, N.; Grätzel, C.; Zakeeruddin, S. M.; Röthlisberger, U.; Grätzel, M. Entropic Stabilization of Mixed A-Cation ABX 3 Metal Halide Perovskites for High Performance Perovskite Solar Cells. *Energy Environ. Sci.* **2016**, *9*, 656−662.

(11) Kagan, C. R.; Mitzi, D. B.; Dimitrakopoulos, C. D. Organic-Inorganic Hybrid Materials as Semiconducting Channels in Thin-Film Field-Effect Transistors. *Science* **1999**, *286*, 945−947.

(12) Chen, Y.; Chen, T.; Dai, L. Layer-by-layer Growth of CH3NH3PbI3− XClx for Highly Efficient Planar Heterojunction Perovskite Solar Cells. *Adv. Mater.* **2015**, *27*, 1053−1059.

(13) Smith, I. C.; Hoke, E. T.; Solis-Ibarra, D.; McGehee, M. D.; Karunadasa, H. I. A Layered Hybrid Perovskite Solar-cell Absorber with Enhanced Moisture Stability. *Angew. Chem.* **2014**, *126*, 11414−11417.

(14) Quan, L. N.; Yuan, M.; Comin, R.; Voznyy, O.; Beauregard, E. M.; Hoogland, S.; Buin, A.; Kirmani, A. R.; Zhao, K.; Amassian, A.; Kim, D. H.; Sargent, E. H. Ligand-Stabilized Reduced-Dimensionality Perovskites. *J. Am. Chem. Soc.* **2016**, *138*, 2649−2655.

(15) Kim, H.-S.; Lee, C.-R.; Im, J.-H.; Lee, K.-B.; Moehl, T.; Marchioro, A.; Moon, S.-J.; Humphry-Baker, R.; Yum, J.-H.; Moser, J. E. Lead Iodide Perovskite Sensitized All-Solid-State Submicron Thin Film Mesoscopic Solar Cell with Efficiency Exceeding 9. *Sci. Rep.* **2012**, *2*, 591.

(16) Misra, R. K.; Aharon, S.; Li, B.; Mogilyansky, D.; Visoly-Fisher, I.; Etgar, L.; Katz, E. A. Temperature-and Component-Dependent Degradation of Perovskite Photovoltaic Materials under Concentrated Sunlight. *J. Phys. Chem. Lett.* **2015**, *6*, 326−330.

(17) Eperon, G. E.; Stranks, S. D.; Menelaou, C.; Johnston, M. B.; Herz, L. M.; Snaith, H. J. Formamidinium Lead Trihalide: A Broadly Tunable Perovskite for Efficient Planar Heterojunction Solar Cells. *Energy Environ. Sci.* **2014**, *7*, 982−988.

(18) Yang, J.; Siempelkamp, B. D.; Liu, D.; Kelly, T. L. Investigation of CH3NH3PbI3 Degradation Rates and Mechanisms in Controlled Humidity Environments Using in Situ Techniques. *ACS Nano* **2015**, *9*, 1955−1963.

(19) You, J.; Meng, L.; Song, T.-B.; Guo, T.-F.; Yang, Y.; Chang, W.-H.; Hong, Z.; Chen, H.; Zhou, H.; Chen, Q.; Liu, Y.; De Marco, N.; Yang, Y. Improved Air Stability of Perovskite Solar Cells via Solution-Processed Metal Oxide Transport Layers. *Nat. Nanotechnol.* **2016**, *11*, 75−81.

(20) Snaith, H. J.; Abate, A.; Ball, J. M.; Eperon, G. E.; Leijtens, T.; Noel, N. K.; Stranks, S. D.; Wang, J. T.-W.; Wojciechowski, K.; Zhang, W. Anomalous Hysteresis in Perovskite Solar Cells. *J. Phys. Chem. Lett.* **2014**, *5*, 1511−1515.

(21) Tiep, N. H.; Ku, Z.; Fan, H. J. Recent Advances in Improving the Stability of Perovskite Solar Cells. *Adv. Energy Mater.* **2016**, *6*, 1501420−150142.

(22) Bi, D.; Boschloo, G.; Schwarzmüller, S.; Yang, L.; Johansson, E. M. J.; Hagfeldt, A. Efficient and Stable CH 3 NH 3 PbI 3-Sensitized ZnO Nanorod Array Solid-State Solar Cells. *Nanoscale* **2013**, *5*, 11686−11691.

(23) Mahmood, K.; Swain, B. S.; Amassian, A. 16.1% Efficient Hysteresis-free Mesostructured Perovskite Solar Cells Based on Synergistically Improved ZnO Nanorod Arrays. *Adv. Energy Mater.* **2015**, *5*, 1500568.

(24) Wojciechowski, K.; Leijtens, T.; Siprova, S.; Schlueter, C.; Hörantner, M. T.; Wang, J. T.-W.; Li, C.-Z.; Jen, A. K.-Y.; Lee, T.-L.; Snaith, H. J. C60 as an Efficient N-Type Compact Layer in Perovskite Solar Cells. *J. Phys. Chem. Lett.* **2015**, *6*, 2399−2405.

(25) Heo, J. H.; Shin, D. H.; Jang, M. H.; Lee, M. L.; Kang, M. G.; Im, S. H. Highly flexible, high-performance perovskite solar cells with adhesion promoted AuCl3-doped graphene electrodes. *J. Mater. Chem. A* **2017**, *5*, 21146−21152.

(26) Yu, Z.; Sun, L. Recent Progress on Hole-transporting Materials for Emerging Organometal Halide Perovskite Solar Cells. *Adv. Energy Mater.* **2015**, *5*, 1500213.
(27) Bakr, Z. H.; Wali, Q.; Fakharuddin, A.; Schmidt-Mende, L.; Brown, T. M.; Jose, R. Advances in Hole Transport Materials Engineering for Stable and Efficient Perovskite Solar Cells. *Nano Energy* **2017**, *34*, 271−305.
(28) Habisreutinger, S. N.; Leijtens, T.; Eperon, G. E.; Stranks, S. D.; Nicholas, R. J.; Snaith, H. J. Carbon Nanotube/Polymer Composites as a Highly Stable Hole Collection Layer in Perovskite Solar Cells. *Nano Lett.* **2014**, *14*, 5561−5568.
(29) Xie, H.; Lira-Cantu, M. Multi-Component Engineering to Enable Long-Term Operational Stability of Perovskite Solar Cells. *J. Phys. Energy* **2020**, *2*, 24008.
(30) Fu, Q.; Tang, X.; Huang, B.; Hu, T.; Tan, L.; Chen, L.; Chen, Y. Recent Progress on the Long-term Stability of Perovskite Solar Cells. *Adv. Sci.* **2018**, *5*, 1700387.
(31) Wu, X.; Xie, L.; Lin, K.; Lu, J.; Wang, K.; Feng, W.; Fan, B.; Yin, P.; Wei, Z. Efficient and Stable Carbon-Based Perovskite Solar Cells Enabled by the Inorganic Interface of CuSCN and Carbon Nanotubes. *J. Mater. Chem. A* **2019**, *7*, 12236−12243.
(32) Kung, P.-K.; Li, M.; Lin, P.; Chiang, Y.; Chan, C.; Guo, T.; Chen, P. A Review of Inorganic Hole Transport Materials for Perovskite Solar Cells. *Adv. Mater. Interfaces* **2018**, *5*, 1800882.
(33) Lin, Y.; Bai, Y.; Fang, Y.; Chen, Z.; Yang, S.; Zheng, X.; Tang, S.; Liu, Y.; Zhao, J.; Huang, J. Enhanced Thermal Stability in Perovskite Solar Cells by Assembling 2D/3D Stacking Structures. *J. Phys. Chem. Lett.* **2018**, *9*, 654−658.
(34) Li, W.; Lai, X.; Meng, F.; Li, G.; Wang, K.; Kyaw, A. K. K.; Sun, X. W. Efficient Defect-Passivation and Charge-Transfer with Interfacial Organophosphorus Ligand Modification for Enhanced Performance of Perovskite Solar Cells. *Sol. Energy Mater. Sol. Cells* **2020**, *211*, 110527.
(35) Kakavelakis, G.; Paradisanos, I.; Paci, B.; Generosi, A.; Papachatzakis, M.; Maksudov, T.; Najafi, L.; Del Rio Castillo, A. E.; Kioseoglou, G.; Stratakis, E. Extending the Continuous Operating Lifetime of Perovskite Solar Cells with a Molybdenum Disulfide Hole Extraction Interlayer. *Adv. Energy Mater.* **2018**, *8*, 1702287.
(36) Capasso, A.; Matteocci, F.; Najafi, L.; Prato, M.; Buha, J.; Cinà, L.; Pellegrini, V.; Carlo, A. D.; Bonaccorso, F. Few-Layer MoS2 Flakes as Active Buffer Layer for Stable Perovskite Solar Cells. *Adv. Energy Mater.* **2016**, *6*, 1600920.
(37) Dai, R.; Wang, Y.; Wang, J.; Deng, X. Metal−Organic-compound-modified MoS2 with Enhanced Solubility for High-performance Perovskite Solar Cells. *ChemSusChem* **2017**, *10*, 2869−2874.
(38) Wang, D.; Elumalai, N. K.; Mahmud, M. A.; Yi, H.; Upama, M. B.; Lee Chin, R. A.; Conibeer, G.; Xu, C.; Haque, F.; Duan, L.; Uddin, A. MoS2 Incorporated Hybrid Hole Transport Layer for High Performance and Stable Perovskite Solar Cells. *Synth. Met.* **2018**, *246*, 195−203.
(39) Najafi, L.; Taheri, B.; Martín-García, B.; Bellani, S.; Di Girolamo, D.; Agresti, A.; Oropesa-Nuñez, R.; Pescetelli, S.; Vesce, L.; Calabrò, E.; Prato, M.; Del Rio Castillo, A. E.; Di Carlo, A.; Bonaccorso, F. MoS2 Quantum Dot/Graphene Hybrids for Advanced Interface Engineering of a CH3NH3PbI3 Perovskite Solar Cell with an Efficiency of over 20. *ACS Nano* **2018**, *12*, 10736−10754.
(40) Khenkin, M. V.; Katz, E. A.; Abate, A.; Bardizza, G.; Berry, J. J.; Brabec, C.; Brunetti, F.; Bulović, V.; Burlingame, Q.; Di Carlo, A.; Cheacharoen, R.; Cheng, Y.-B.; Colsmann, A.; Cros, S.; Domanski, K.; Dusza, M.; Fell, C. J.; Forrest, S. R.; Galagan, Y.; Di Girolamo, D.; Grätzel, M.; Hagfeldt, A.; von Hauff, E.; Hoppe, H.; Kettle, J.; Köbler, H.; Leite, M. S.; Liu, S.; Loo, Y.-L.; Luther, J. M.; Ma, C.-Q.; Madsen, M.; Manceau, M.; Matheron, M.; McGehee, M.; Meitzner, R.; Nazeeruddin, M. K.; Nogueira, A. F.; Odabaşı, Ç.; Osherov, A.; Park, N.-G.; Reese, M. O.; De Rossi, F.; Saliba, M.; Schubert, U. S.; Snaith, H. J.; Stranks, S. D.; Tress, W.; Troshin, P. A.; Turkovic, V.; Veenstra, S.; Visoly-Fisher, I.; Walsh, A.; Watson, T.; Xie, H.; Yıldırım, R.; Zakeeruddin, S. M.; Zhu, K.; Lira-Cantu, M. Consensus Statement for Stability Assessment and Reporting for Perovskite Photovoltaics Based on ISOS Procedures. *Nat. Energy* **2020**, *5*, 35−49.
(41) Sherkar, T. S.; Momblona, C.; Gil-Escrig, L.; Ávila, J.; Sessolo, M.; Bolink, H. J.; Koster, L. J. A. Recombination in Perovskite Solar Cells: Significance of Grain Boundaries, Interface Traps, and Defect Ions. *ACS Energy Lett.* **2017**, *2*, 1214−1222.
(42) Weber, S. A. L.; Hermes, I. M.; Turren-Cruz, S.-H.; Gort, C.; Bergmann, V. W.; Gilson, L.; Hagfeldt, A.; Graetzel, M.; Tress, W.; Berger, R. How the Formation of Interfacial Charge Causes Hysteresis in Perovskite Solar Cells. *Energy Environ. Sci.* **2018**, *11*, 2404−2413.
(43) Singh, R.; Sandhu, S.; Lee, J.-J. Elucidating the Effect of Shunt Losses on the Performance of Mesoporous Perovskite Solar Cells. *Sol. Energy* **2019**, *193*, 956−961.
(44) Almora, O.; Aranda, C.; Mas-Marzá, E.; Garcia-Belmonte, G. On Mott-Schottky Analysis Interpretation of Capacitance Measurements in Organometal Perovskite Solar Cells. *Appl. Phys. Lett.* **2016**, *109*, 173903.
(45) Calado, P.; Telford, A. M.; Bryant, D.; Li, X.; Nelson, J.; O'Regan, B. C.; Barnes, P. R. F. Evidence for Ion Migration in Hybrid Perovskite Solar Cells with Minimal Hysteresis. *Nat. Commun.* **2016**, *7*, 13831.
(46) Gottesman, R.; Lopez-Varo, P.; Gouda, L.; Jimenez-Tejada, J. A.; Hu, J.; Tirosh, S.; Zaban, A.; Bisquert, J. Dynamic Phenomena at Perovskite/Electron-Selective Contact Interface as Interpreted from Photovoltage Decays. *Chem* **2016**, *1*, 776−789.
(47) Gelmetti, I.; Montcada, N. F.; Pérez-Rodríguez, A.; Barrena, E.; Ocal, C.; García-Benito, I.; Molina-Ontoria, A.; Martín, N.; Vidal-Ferran, A.; Palomares, E. Energy Alignment and Recombination in Perovskite Solar Cells: Weighted Influence on the Open Circuit Voltage. *Energy Environ. Sci.* **2019**, *12*, 1309−1316.
(48) Hidayat, R.; Nurunnizar, A. A.; Fariz, A.; Herman, E. S.; Rosa, E. S.; Shobih, A.; Oizumi, T.; Fujii, A.; Ozaki, M. Revealing the Charge Carrier Kinetics in Perovskite Solar Cells Affected by Mesoscopic Structures and Defect States from Simple Transient Photovoltage Measurements. *Sci. Rep.* **2020**, *10*, 19197.
(49) Chen, X.; Shirai, Y.; Yanagida, M.; Miyano, K. Effect of Light and Voltage on Electrochemical Impedance Spectroscopy of Perovskite Solar Cells: An Empirical Approach Based on Modified Randles Circuit. *J. Phys. Chem. C* **2019**, *123*, 3968−3978.
(50) Bou, A.; Pockett, A.; Raptis, D.; Watson, T.; Carnie, M. J.; Bisquert, J. Beyond Impedance Spectroscopy of Perovskite Solar Cells: Insights from the Spectral Correlation of the Electrooptical Frequency Techniques. *J. Phys. Chem. Lett.* **2020**, *11*, 8654−8659.
(51) Ebadi, F.; Taghavinia, N.; Mohammadpour, R.; Hagfeldt, A.; Tress, W. Origin of Apparent Light-Enhanced and Negative Capacitance in Perovskite Solar Cells. *Nat. Commun.* **2019**, *10*, 1574.
(52) Ghahremanirad, E.; Bou, A.; Olyaee, S.; Bisquert, J. Inductive Loop in the Impedance Response of Perovskite Solar Cells Explained by Surface Polarization Model. *J. Phys. Chem. Lett.* **2017**, *8*, 1402−1406.
(53) Albadri, A.; Yadav, P.; Alotaibi, M.; Arora, N.; Alyamani, A.; Albrithen, H.; Dar, M. I.; Zakeeruddin, S. M.; Grätzel, M. Unraveling the Impact of Rubidium Incorporation on the Transport-Recombination Mechanisms in Highly Efficient Perovskite Solar Cells by Small-Perturbation Techniques. *J. Phys. Chem. C* **2017**, *121*, 24903−24908.
(54) Tress, W. Metal Halide Perovskites as Mixed Electronic−Ionic Conductors: Challenges and Opportunities— From Hysteresis to Memristivity. *J. Phys. Chem. Lett.* **2017**, *8*, 3106−3114.
(55) Wolff, C. M.; Caprioglio, P.; Stolterfoht, M.; Neher, D. Nonradiative Recombination in Perovskite Solar Cells: The Role of Interfaces. *Adv. Mater.* **2019**, *31*, 1902762.
(56) Senanayak, S. P.; Abdi-Jalebi, M.; Kamboj, V. S.; Carey, R.; Shivanna, R.; Tian, T.; Schweicher, G.; Wang, J.; Giesbrecht, N.; Di Nuzzo, D.; Beere, H. E.; Docampo, P.; Ritchie, D. A.; Fairen-Jimenez, D.; Friend, R. H.; Sirringhaus, H. A General Approach for Hysteresis-Free, Operationally Stable Metal Halide Perovskite Field-Effect Transistors. *Sci. Adv.* **2020**, *6*, No. eaaz4948.

https://doi.org/10.1021/acsaem.1c02412
ACS Appl. Energy Mater. 2021, 4, 14080−14092

(57) Santos, E. J. G.; Kaxiras, E. Electrically Driven Tuning of the Dielectric Constant in MoS2 Layers. *ACS Nano* **2013**, *7*, 10741−10746.
(58) Ebadi, F.; Aryanpour, M.; Mohammadpour, R.; Taghavinia, N. Coupled Ionic-Electronic Equivalent Circuit to Describe Asymmetric Rise and Decay of Photovoltage Profile in Perovskite Solar Cells. *Sci. Rep.* **2019**, *9*, 11962.
(59) Klotz, D. Negative Capacitance or Inductive Loop?−A General Assessment of a Common Low Frequency Impedance Feature. *Electrochem. Commun.* **2019**, *98*, 58−62.
(60) Wang, Q. Influence of a Cobalt Additive in Spiro-OMeTAD on Charge Recombination and Carrier Density in Perovskite Solar Cells Investigated Using Impedance Spectroscopy. *Phys. Chem. Chem. Phys.* **2018**, *20*, 10114−10120.

https://doi.org/10.1021/acsaem.1c02412
ACS Appl. Energy Mater. 2021, 4, 14080−14092